

Simulation of a Casimir-like effect in a granular pile with avalanches

D. V. Denisov, Y. Y. Villanueva, and R. J. Wijngaarden

Department of Physics, Faculty of Sciences, VU University Amsterdam, De Boelelaan 1081, NL-1081 HV Amsterdam, The Netherlands

(Received 17 January 2011; revised manuscript received 20 April 2011; published 22 June 2011)

Using a modified Bak-Tang-Wiesenfeld model for sand piles, we simulate a Casimir-like effect in a granular pile with avalanches. Results obtained in the simulation are in good agreement with results previously acquired experimentally: two parallel walls are attracted to each other at small separation distances, with a force decreasing with increasing distance. In the simulation only, at medium distances a weak repulsion exists. Additionally, with the aim of avalanche prevention, the possibility of suppressing self-organized criticality with an array of walls placed on the slope of the pile is investigated, but the prevention effect is found to be negligible.

DOI: [10.1103/PhysRevE.83.061301](https://doi.org/10.1103/PhysRevE.83.061301)

PACS number(s): 45.70.Ht, 05.65.+b

I. INTRODUCTION

For quite a long time, scientists have studied the phenomenon of self-organized criticality (SOC) [1], which manifests itself in various processes: earthquakes [2], landslides [3], forest fires [4], rice piles [5], magnetic avalanches in superconductors [6], evolutionary bursts [7], financial markets [8], etc. In a SOC system, energy is added to the system at a low rate, leading to an accumulation of instability. This instability is later released in an abrupt event, usually called an avalanche. These avalanches have a probability density that is a power law. Hence, there are avalanches of all sizes, and some of them can be very large and devastating. Many attempts have been undertaken to control avalanches, but SOC behavior has proven to be very hard to suppress.

In the Casimir effect [9] two parallel conducting plates are driven together because, put simply, long-wavelength electromagnetic vacuum fluctuations are suppressed between them. Since a SOC system with its avalanches is a fluctuating system with fluctuations on all scales, one may expect Casimir-like effects. Indeed, recent experiments on a rice pile with two parallel sheets placed along the mean avalanche flow confirm the existence of such a Casimir-like effect [10] in a granular system with avalanches. Due to the fluctuations in the form of avalanches, the two sheets experience a net attractive force, and move closer to each other in the course of the experiment. In addition, it was noted that the slope of the pile between the sheets is notably steeper than in the rest of the pile, which could offer possibilities for the control of avalanche flow.

To model avalanching granular systems Bak, Tang, and Wiesenfeld [11] (BTW) created a simple numerical model, that has been used extensively. Since the original BTW model simulates the behavior of local slopes, and does not allow (in dimension larger than 1) the extraction of the local heights, we have developed a modified model enabling the simulation of the full three-dimensional shape of a rice pile, thus enabling a direct comparison with the experiments of Ref. [10]. By placing two parallel walls in our simulated pile and by carefully studying their interaction with passing particles, we reproduce the results obtained in the experiment. Apart from the attraction of two walls at small distances we find a weak repulsion between them at medium distances. In addition, we have investigated the possibility of controlling the avalanches (in our model), with the help of the Casimir-like effect, by placing an array of walls on the slope of the pile.

In Sec. II, details of our modified BTW model are given. In Sec. III, we present results of more than 100 simulation runs reproducing the experimental Casimir-like effect. In Sec. IV, we compare the experimental and numerical results for the dependence of the magnitude of the Casimir-like force on the initial separation distance. In Sec. V, we show the effect of placing an array of walls on the slope of the pile to try and prevent avalanche propagation. Final conclusions are presented in Sec. VI.

II. HEIGHT MODEL

To simulate self-organized criticality in granular materials, the model of Bak, Tang, and Wiesenfeld [11] has been widely used. Indeed, the size distribution of the avalanches that can be triggered in the two-dimensional BTW model follows a power law $P(s) \sim s^{-\tau_{BTW}}$, with τ_{BTW} close to 1.0 [11]. In the original BTW model the avalanching process is organized as follows. Each site (x, y) on a rectangular grid has a slope value z . If z exceeds a critical threshold K , the following update on the site and its nearest neighbors occurs:

$$\begin{aligned} z(x, y) &\rightarrow z(x, y) - 4, \\ z(x \pm 1, y) &\rightarrow z(x \pm 1, y) + 1, \\ z(x, y \pm 1) &\rightarrow z(x, y \pm 1) + 1. \end{aligned} \quad (1)$$

If, after the update, the neighboring site also exceeds the threshold K , another toppling will occur, possibly involving more sites in the process, which will continue until all sites are in a stable state. The size of an avalanche is calculated as the total number of particle motions involved in the process before everything stabilizes [11]. To create another avalanche, the z coordinate of one of the sites (fixed or random) is increased by 1 and checked again for exceeding the threshold. This simple model shows the basics of avalanche creation and dynamics, but it cannot reproduce real avalanche behavior in granular piles. First of all, the toppling condition for each site is checked against a universal constant K rather than comparing the relative heights of all neighboring site. Because of this, the z coordinate represents the local slope of the pile rather than its local height. Second, all sites topple in a uniform way, leading to a deterministic or Abelian process which creates avalanches with a “mosaiclike” shape. From a two-dimensional slope model, one cannot make a transformation to height values

of the pile (although the inverse transformation is possible). For these reasons, slope models cannot exactly represent real avalanches.

Our goal here is to change the BTW model in such a way that it can reproduce the shape of real sand piles and of real avalanches. This is implemented by having the z coordinate representing the *height* of the pile instead of its *slope*. Let us designate the new value of the height as a variable h , while the variable z represents the slope. If we have only a one-dimensional model then simply $z_n = h(n) - h(n + 1)$ (where n is a coordinate in one-dimensional space), as was introduced in the well-established cellular automaton model [11]. However, for the two-dimensional model that we will use in the present paper we make several changes. First, we change from four to eight nearest neighbors, since we want to introduce more degrees of freedom for the particle motion, so that it will be closer to the grain motion in a real sand pile. Second, we do not simultaneously move particles along the x and y directions when a certain threshold for the slope is reached. Instead (see Fig. 1), when the difference in h for two sites along one direction exceeds a threshold K_{\max} the particles start to topple but will move only to the neighboring sites which have h lower than the central toppling site. The number of toppling directions could be different for each individual process (ranging from 1 to 8). Additionally, several particles could topple along the same direction if the difference in h between neighboring sites for this direction was large in the beginning of the toppling process [see, for example, case (a) in Fig. 1]. The condition to start the toppling process at least

along one direction for a given site $h(x, y)$ is given by the following expression:

$$\text{OR} \begin{cases} h(x, y) - h(x \pm 1, y \pm 1) \geq K_{\max}, \\ h(x, y) - h(x, y \pm 1) \geq K_{\max}, \\ h(x, y) - h(x \pm 1, y) \geq K_{\max}. \end{cases} \quad (2)$$

To stop the toppling process, we need a lower threshold K_{\min} . If the difference in h along one direction becomes smaller than the value K_{\min} , then the toppling along this direction will stop. If the difference in h is smaller than the value K_{\min} along all eight directions, then the toppling process stops and the central site is considered stable. The main difference from the BTW model is that the number of particles participating in each toppling process is not *a priori* specified, but is determined by the starting condition (2) and the following stopping condition:

$$\text{AND} \begin{cases} h(x, y) - h(x \pm 1, y \pm 1) < K_{\min}, \\ h(x, y) - h(x, y \pm 1) < K_{\min}, \\ h(x, y) - h(x \pm 1, y) < K_{\min}. \end{cases} \quad (3)$$

During the toppling process the particles are distributed randomly to the allowed (lower) neighbor sites. This is an essential difference with respect to the BTW model, which is completely deterministic. Due to the randomness in distributing particles, even for the same initial conditions each toppling sequence can be different; see Fig. 1. Moreover, even for the same initial conditions the number of toppling particles from the central site can be different, as shown, for example, in cases (d) and (e) in Fig. 1.

Note that our model cannot be directly compared to the Manna model [12], where during the toppling process a definite number of particles is distributed to the neighboring sites in a completely random way. In our case, the directions for toppling are not chosen completely randomly, but only from a set of allowed directions. Additionally, as already mentioned, the number of distributed particles during each process is not fixed.

Each site topples until it is in a completely stable state and condition (3) is fulfilled; for example, as shown in the final diagrams in Fig. 1. It should be noted that an update due to the toppling occurs simultaneously for all sites in the pile (parallel update). Each update may give rise to an instability on neighboring sites, resulting in new topplings and another system-wide check according to Eqs. (2) and (3). This procedure is repeated until all sites become stable. We define as one avalanche all events happening after the first site becomes unstable until all sites are stable again. The number of updates needed to stabilize the entire system after the first toppling is defined as the duration of the avalanche. For SOC behavior, the system must be in the slow-driving regime [13]. Hence, only one particle at a time is added to the pile and no particles are added during the avalanche evolution. Our model reproduces closely the shape of the real granular pile as well as the corresponding avalanches; see Fig. 2.

For the computation, a lattice of 100×150 sites is used to represent a half-closed box with high walls; only the front edge at $y = 0$ remains open, where particles can leave the box (Fig. 3). In the figure, the z axis was multiplied by 0.3 to obtain a more realistic look of the initial pile with angle close to 30° , as in the experiment. The pile initially occupies a region of 100×100 sites, with a uniform slope and maximum height at

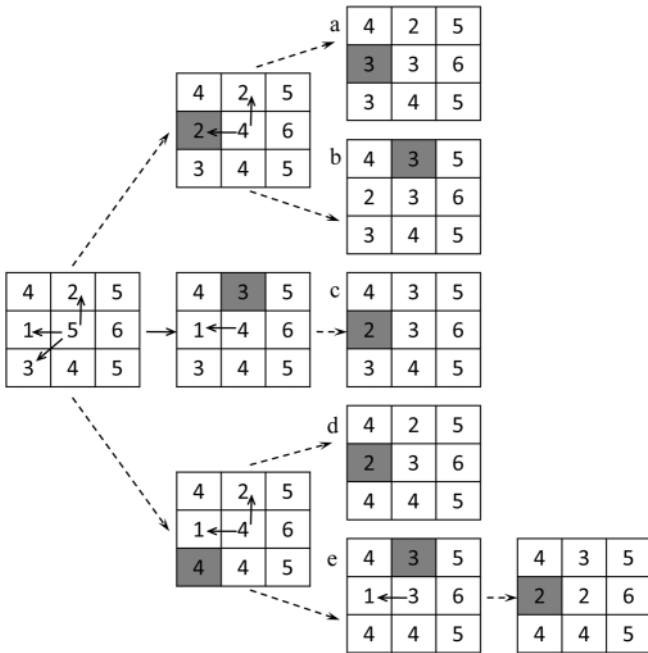


FIG. 1. Examples of the toppling process from the central site to the eight nearest neighbors (with $K_{\max} = 3$, $K_{\min} = 2$; see text). The numbers represent the number of particles in that site. Arrows inside squares indicate possible ways for the particle to move during the next step. Dark squares show the sites to which the particles have moved. In cases (a)–(d) two particles toppled from the central site but in the case (e) three.

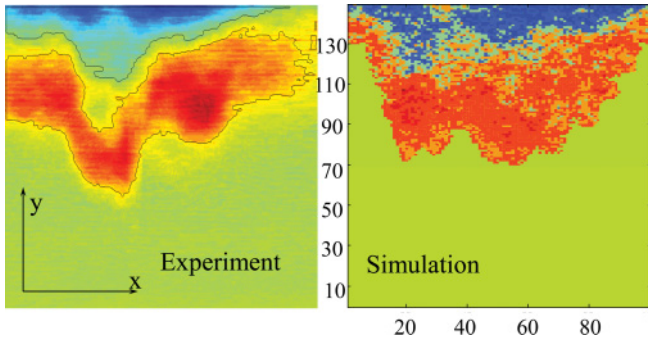


FIG. 2. (Color online) Images of two typical avalanches. Left: an experimentally observed avalanche in our rice pile. Right: an avalanche as obtained by the present simulation. Blue (upper dark gray part of the image) indicates regions where particles are removed, and red (lower part of the image) indicates regions where particles are added.

the back edge of the simulation “box.” New particles are added at this very edge uniformly and randomly across its whole length (each new particle locally increase the value of h by 1). A region of 50×100 sites at the foot of the pile is initially left unoccupied to ensure that during the simulation there is enough space for the pile to grow without any particles leaving the system, in order to exactly reproduce the experiment presented in [10].

To calculate the size of the avalanches s occurring in our simulation, we can use two methods of avalanche counting. If we define s as the number of particle motions during avalanche propagation, as is done in the original BTW simulations, then we get the avalanche size distribution $P(s) \sim s^{-\tau_p}$ with τ_p close to 1.64; see Fig. 4(a).

The value of $\tau_p \simeq 1.64$ obtained in our simulation is higher than reported in most other simulations, notably in two-dimensional BTW-like models, where the value of the exponent is close to 1.0. We now discuss the reasons for this.

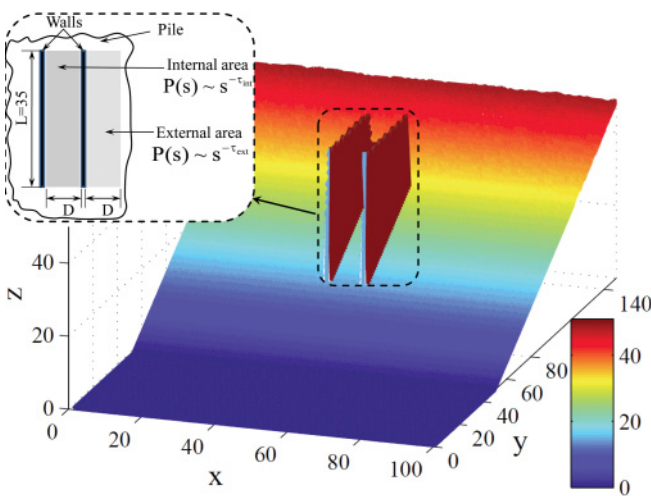


FIG. 3. (Color online) Schematic of the simulated pile. The pile is surrounded by high walls at three sides (at $x = 0$, $x = 100$, and $y = 150$) and particles can only leave the pile at the front ($y = 0$). Two parallel walls are placed in the middle of the pile. Inset: the internal and external areas near the walls that we used in our calculations.

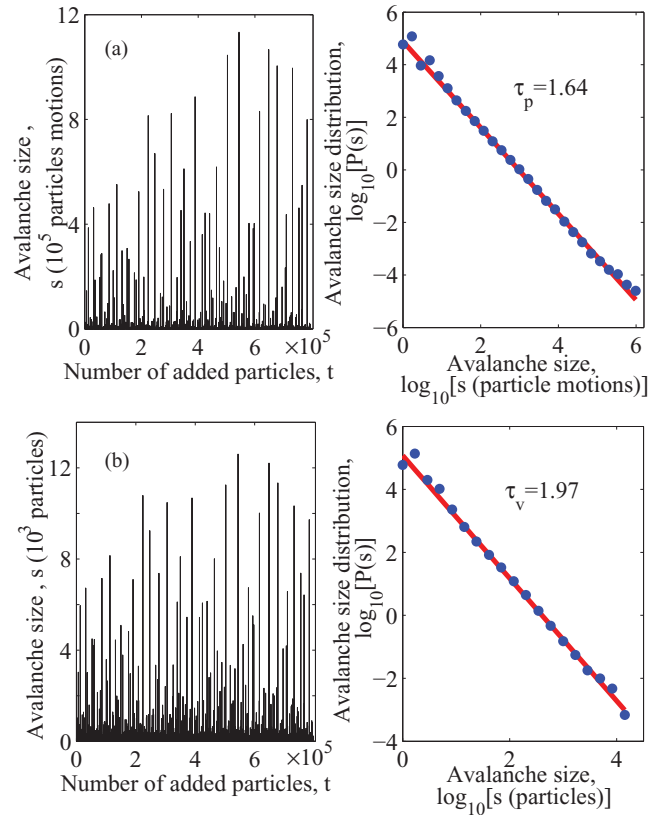


FIG. 4. (Color online) (a) Avalanche sizes for the particle motion counting method. Left: size of avalanches versus number of added particles (time). Right: the corresponding avalanche size distribution, which is a power law $P(s) \sim s^{-\tau_p}$ with $\tau_p \simeq 1.64$. (b) Avalanche sizes for the surface subtraction method. Left: size of avalanches versus number of added particles (time). Right: the corresponding avalanche size distribution, which is a power law $P(s) \sim s^{-\tau_v}$ with $\tau_v = 1.97$. The plots in (a) and (b) are based on data from the same simulation. Simulation data points are shown by blue circles and the red solid line is a power-law fit.

First, we use a height model rather than a slope model, and in the two-dimensional case a general mapping from slopes to heights is impossible. While in the two-dimensional BTW model each site is characterized by a single slope value, our toppling rules take into account eight different slope values at each site (the differences between the site and its closest neighbors). This creates an effective higher dimensionality, and it is known that a higher dimensionality usually leads to higher values of τ [14]. Second, in contrast to the BTW models we introduced randomness to our toppling rules, and it is known that randomness usually leads to an increase of τ , as shown, e.g., by Manna [12] and Christensen *et al.* [15]. Third, we add new grains only at the top of the pile, in contrast to the random seeding across the whole pile by BTW, and it is known that seeding at the top only can lead to much larger values of τ ; e.g., Bengrine *et al.* reported [16] $\tau = 1.53$, which is rather close to our result $\tau_p = 1.64$.

Up to now we have discussed the values of τ as the number of particle motions during avalanche propagation, as is done in the original BTW simulations. In our *experiments* on a real rice pile (Ref. [10]), this counting method is not possible due

to the rapid progression of avalanches. Instead, we subtract the pile surfaces before and after an avalanche, thus finding the net change in height for each position. We define the size of the avalanche s as the sum of all positive changes in height. This means that we count only displaced particles (if no particles leave the pile during the avalanche then the positive and negative parts of the profile subtraction are equal). In this case, s thus represent the volume of the avalanche, which is proportional to the number of particles in the avalanche. If this method is used to define the avalanche size of our *simulations*, we find a power-law size distribution $P(s) \sim s^{-\tau_v}$, with $\tau_v \simeq 2$. Hence changing from counting particle motions to counting avalanche volume changes the exponent from $\tau_p = 1.64$ to $\tau_v = 1.97$ [see Fig. 4(b)].

We used several sets of reasonable values of the constants $K_{\max} > K_{\min} \geq 2$ and it was found that the avalanche size distribution is always a power law, with τ independent of K_{\max}, K_{\min} for both methods of size calculation. For the simulations presented below, we chose $K_{\max} = 3$ and $K_{\min} = 2$ and defined the avalanche size s from subtraction of surfaces (as in the experiments [10]). Consistent with this, we denote the power-law distribution exponent by τ_v . The size s of the avalanches in our simulation varies from 2 particles (minimum possible avalanche) to around 2×10^4 (system-wide avalanches, covering several layers of particles); for a typical result, see Fig. 4(b).

III. CASIMIR-LIKE EFFECT

It was recently discovered that a Casimir-like effect can be observed in an avalanching granular pile [10]. In that work, an attractive force was observed between two parallel Plexiglas sheets placed initially at 3–9 cm distance from each other in the pile of rice. When grains were slowly added at the top of the rice pile, avalanches occurred with a size varying from a few grains to system-wide ones. The size distribution of these avalanches follows a power law $P(s) \sim s^{-\tau_{\text{rice}}}$, with $\tau_{\text{rice}} = 1.12$ [17], which indicates SOC behavior. The avalanches act as fluctuations that drive the sheets together, like the electromagnetic fluctuations in the real Casimir effect [9]. The difference between the experimental value τ_{rice} and the simulated value τ_v is probably due to the fact that in the simulation the grains are presented as uniform particles on a square lattice rather than real elongated grains which can form rather complicated scaffolding structures. Despite this difference, the general behavior of the pile is reproduced, with a power-law avalanche size distribution and realistically shaped avalanches [Figs. 2 and 4(b)].

In order to simulate the Casimir-like effect, we placed two walls in the pile to represent the two Plexiglas sheets of the experiment. The walls are two parallel lines of sites in the middle of the pile that are made immobile and unchangeable with height h_l much larger than the rest of the pile and with a length of 35 sites (close to 1/3 of the initial pile length; see Fig. 3). These walls are placed at a distance D from each other, with D varying from 1 to 20 sites for different simulation runs. The height h_l of the walls implies that no particle can come to or leave from the sites of the walls. In contrast to the original experiment, the walls are fixed and cannot move during the simulation. Due to this fact, we will probably achieve a slightly

smaller average attractive force on the walls. This difference is not very significant, since the distance change during a 25-h experiment was less than 10% for initial distances equal to or larger than 4 cm [10].

In our simulation, adding particle number t may or may not give rise to an avalanche (the number of added particles t can be treated as time elapsed). If it does, we define the force $F(t)$ acting on a wall due to this avalanche as the difference in number of interactions with each side of the wall:

$$F(t) = n_{\text{ext}} - n_{\text{int}}, \quad (4)$$

where n_{int} (n_{ext}) is the number of times a particle comes into contact with the inner (outer) side of a wall. The inner sides of the two walls are facing each other. If there is no avalanche after adding particle t , $F(t) = 0$. The forces $F(t)$ may be negative (repulsion) or positive (attraction); see, e.g., the left-hand panel of Fig. 5. We define the cumulative force $F_c(t) = \sum_{t'=1}^t F(t')$, i.e., the sum of all forces from the start of the simulation up to the moment that t particles are added. Thus $F_c(t)$ depends on the number of added particles. The simulations proceed until 8×10^5 particles have been added to the pile.

For $D \leq 4$ repulsive forces become very rare even for large avalanches, which means that most of the avalanches between the walls are suppressed. Because of this suppression, the net effect of all interactions is dictated mostly by particle motion in the outer area, which does not depend on D , leading to more or less the same attractive force for $D \leq 4$ [Fig. 6(a)]. The constant slope of the cumulative force F_c curve indicates that the walls are pushed together with approximately constant pressure. For slightly larger distances, e.g., for $D = 6$ [Fig. 6(b)], more particles start to interact also with the inner edge of the walls. Now the cumulative force $F_c(t)$ curve starts to fluctuate and the pressure starts to fluctuate. For distances $D > 8$ sites, the suppression of avalanches in the inner area vanishes; hence we expect that the effect of attractive and repulsive interaction is the same, resulting in a zero net effect and cumulative force $F_c(t)$ fluctuating around zero. In

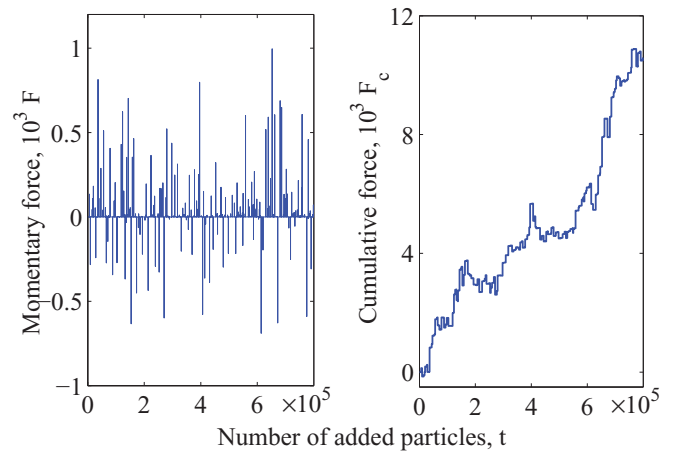


FIG. 5. (Color online) Left: momentary force F acting on the walls versus number of particles t added to the pile (time). Right: cumulative force F_c that has acted on the walls prior to adding a given number of particles (prior to a given time). This cumulative force F_c would correspond to a net motion of the walls, if they could move. The distance between the walls is $D = 6$ pixels.

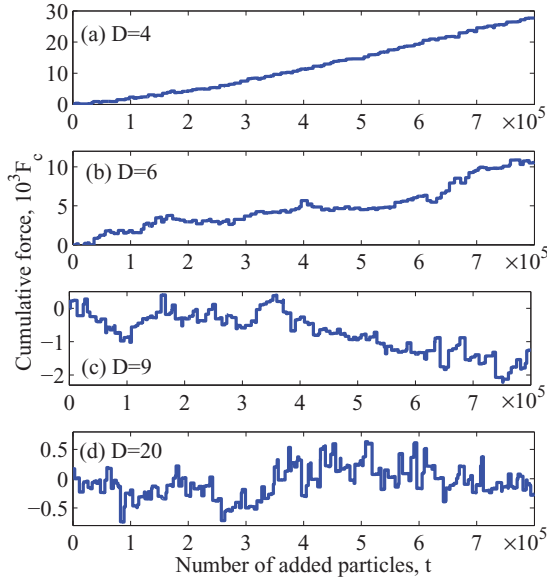


FIG. 6. (Color online) Cumulative force F_c dependence on number of added particles t (time). Results are shown for the wall separations (a) $D = 4$, (b) $D = 6$, (c) $D = 9$, and (d) $D = 20$.

fact, such behavior was observed; however, the average of the fluctuations is slightly below zero, implying a small net repelling force [Fig. 6(c)]. Such behavior was not clearly observed in the experiment (although it also cannot be ruled out completely). We might explain this effect using the fact that for $D \geq 8$ rather big avalanches can move between the walls. During their propagation, such avalanches are “bouncing” between the left and right walls, thus leading to a small repulsion. In the simulation, we took care that the entire pile width is much larger than any considered value of D so that similar bouncing could not happen in the outer region. The bouncing effect very slowly weakens with further increase of D . For example, for $D = 20$ real fluctuations around zero are observed [see Fig. 6(d)]. Overall, the repulsion at large D is much smaller than the Casimir-like attraction observed for $D \leq 8$, meaning that it may be very hard to detect the repulsion experimentally.

We define $F_c^{\text{end}} = F_c(t = 8 \times 10^5)$, i.e., the cumulative force at the end of our simulation runs, when 8×10^5 particles have been added. The dependence of F_c^{end} on distance D is shown in Fig. 7 (average of five simulation runs for each point). The plot indicates that $F_c^{\text{end}}(D)$ decreases as the separation between the walls increases. This result resembles the experimental result shown in [10] (inset of Fig. 7).

It should be noted that the simulation curve $F_c^{\text{end}}(D)$ is much steeper than the experimental one $\Delta D(D)$, which is due to several factors. First of all, in the simulation we measure the exact number n of particles interacting with the walls, but in the experiment we measure the net displacement ΔD caused by these interactions. Direct comparison is not possible since we do not know the exact relation between n and ΔD [this is also the reason that $F_c^{\text{end}}(D)$ has been scaled to 1 on the vertical axis for $D \rightarrow 0$ in Fig. 7]. Second (as mentioned above), in the simulation the walls are immobile, while during the experiment they are moving together. In the experiment we thus actually measure a convolution of the real $\Delta D(D)$ with

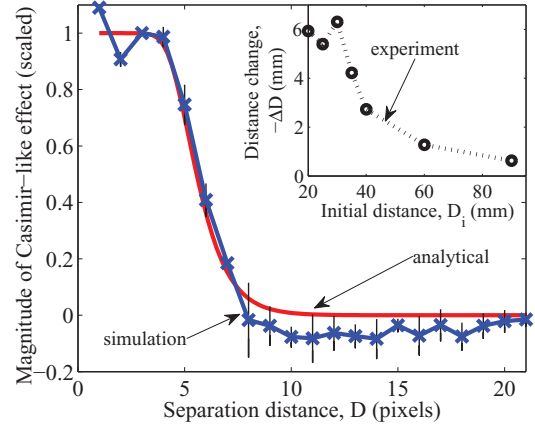


FIG. 7. (Color online) Analytical model (red curve), and simulation data (blue line with crosses) showing the dependence of the Casimir-like effect on the separation distance D between the walls (sheets). All results are scaled to 1 on the vertical axis for $D \rightarrow 0$. Each point on the simulation data curve is the average of five simulation runs; black vertical lines show standard deviation. For comparison, the experimental results from Ref. [10] are shown in the inset.

the change in D , leading to a broadening and resulting in a less steep slope.

To formulate an analytical model for $F_c^{\text{end}}(D)$ (e.g., similar to that in [10]) we should first check that avalanches are really suppressed between the walls and investigate the consequences for the shape of the pile. We average the simulated pile profile in the horizontal direction (along x), but separately for x between and outside the walls. The result is shown in Fig. 8. As in the experiment [10], it is clearly seen that the slope between the walls is steeper. Moreover the profiles do not immediately equalize themselves outside the wall area. Only around 5–10 sites higher and lower than the wall regions do the profiles become even.

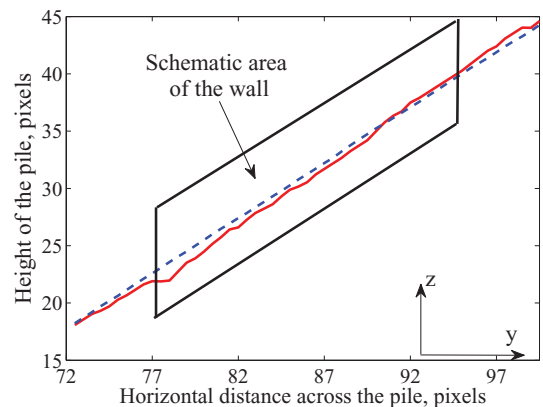


FIG. 8. (Color online) Profile of the slope of the pile between the walls (red solid line) and outside the walls (blue dashed line). Data shown are for the simulation with $D = 4$ pixels, and for 3×10^5 particles added after the start of the experiment. The profile is averaged along x over each region (between the walls and outside the walls) separately.

IV. DISTANCE DEPENDENCE ANALYSIS

To explain the observed steeper slope profile between the walls (or in the experiment sheets), it was suggested in Ref. [10] that the avalanche size distribution in the inner area is different from that in the outer area. In contrast to the experiment, in our simulation we *can* analyze in detail what happens in the area between the walls. In particular, we can monitor the avalanches in this area and the corresponding size distribution $P_{\text{int}}(s)$.

Before doing this we note that the observed size distribution between the walls, $P_{\text{int}}(s)$, is susceptible to distortion, if not corrected for. While the classical BTW model is spatially isotropic because new particles are distributed all over the pile, our model is not: to generate a real pile, new particles are added only at the top of the pile. This might lead to small avalanches occurring predominantly at the top of the pile, while $P_{\text{int}}(s)$ is measured only further down the slope (between the walls). To compensate for this effect and extract the pure effect of the walls on $P(s)$, we compare the behavior in areas of the same size between the walls and outside the walls, with the same width D and the same length and position along y . For example, for $D = 4$ we examine areas of 4×35 sites between the walls and directly outside the walls; see the inset of Fig. 3.

For the external area of $D \times 35$ sites next to the walls, we find $P_{\text{ext}}(s) \sim s^{-\tau_{\text{ext}}}$, with $\tau_{\text{ext}} \approx 0.72$, independent of D . For the internal area for $D = 4$ we find $P_{\text{int}}(s) \sim s^{-\tau_{\text{int}}}$ with the value $\tau_{\text{int}} = 1.31$, implying a significant suppression of large avalanches compared to the outer area. In addition to the difference between τ_{int} and τ_{ext} , the total amount of avalanches occurring between the walls was two times smaller than in the external area (see Figs. 9 and 10). For large D , τ_{int} of course approaches τ_{ext} , leading to the following conjecture:

$$\tau_{\text{int}} = \tau_{\text{ext}} + \tau_0 \exp(-kD), \quad (5)$$

which indeed yields a reasonable heuristic fit in our range of observation for $\tau_0 = 21.59$ and $k = 0.9$.

With these ingredients, a model for the net force can be constructed, in a similar manner as in Ref. [10]. The number

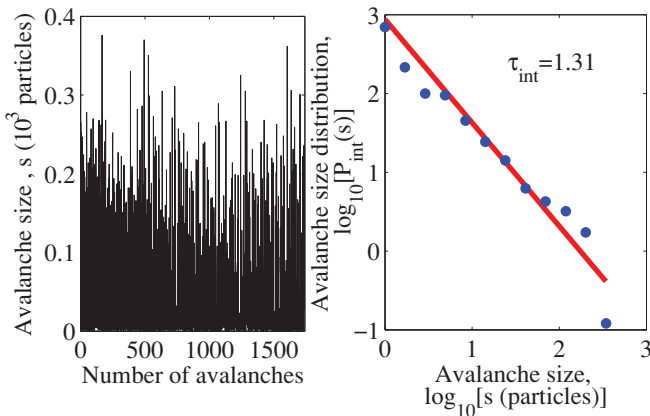


FIG. 9. (Color online) Avalanche size distribution between the walls for $D = 4$. To gather enough statistics the simulation has been performed for a longer time (10^7 particles added). Simulation data points are shown by blue circles and the red solid line is the fit to $P_{\text{int}}(s) \sim s^{-\tau_{\text{int}}}$.

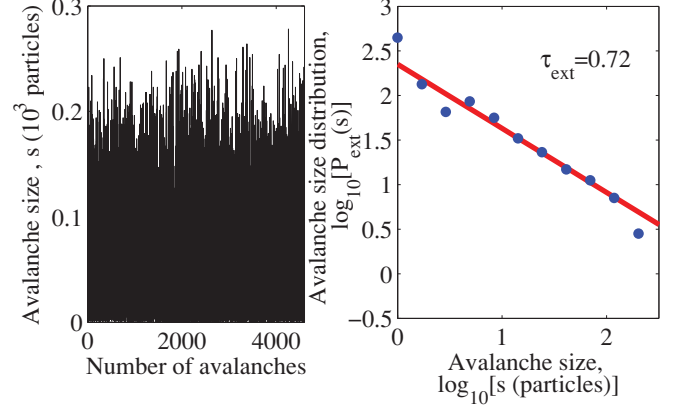


FIG. 10. (Color online) Avalanche size distribution outside the walls for $D = 4$. To gather enough statistics the simulation has been performed for a longer time (10^7 particles added). To be in line with the statistics for the area between the walls, we consider here only avalanches in an area of 4×35 sites directly outside the walls; see text. Simulation data points are shown by blue circles and the red solid line is the fit to $P_{\text{ext}}(s) \sim s^{-\tau_{\text{ext}}}$.

of particles acting on the outside and inside of the walls during the whole duration of a simulation is given by

$$N_{\text{ext}} \sim \int_{s_{\text{min}}}^{s_{\text{max}}} s P_{\text{ext}}(s) ds \quad (6)$$

and

$$N_{\text{int}} \sim \int_{s_{\text{min}}}^{s_{\text{max}}} s P_{\text{int}}(s) ds. \quad (7)$$

Using $F_c = \sum (n_{\text{ext}} - n_{\text{int}}) = N_{\text{ext}} - N_{\text{int}}$ we obtain from $P(s) \sim s^{-\tau}$ and Eqs. (5)–(7)

$$F_c = \beta \int_{s_{\text{min}}}^{s_{\text{max}}} s^{1-\tau_{\text{ext}}} (1 - s^{-\tau_0 \exp(-kD)}) ds, \quad (8)$$

where $s_{\text{min}} = 1$ and s_{max} is the maximum size of an avalanche occurring in the close vicinity of the wall; we choose $s_{\text{max}} = 400$ (the result is insensitive to the exact value of s_{max}). In Fig. 7 we show Eq. (8) as the red smooth curve. Clearly, this analytical model follows very closely the results from the simulation with the exception of a small offset for $D \geq 8$. The small negative force due to the trapping effect is not taken into account nor reproduced by this simple model. Note that the present model reproduces nicely the plateau for $D < 4$ (Fig. 7), in contrast to the analytical model of Ref. [10]. As in Ref. [10], the decaying tail of the analytic model for $5 \leq D \leq 9$ can be fitted to a power law $D^{-\gamma}$ with $\gamma \simeq 4$, while in the experiment [10] $\gamma = 2.6$. Our steeper tail with $\gamma \simeq 4$ is in good agreement with the real Casimir effect [9]; this might, however, be pure coincidence. The difference between simulation and experiment may be due to the convolution of the real $\Delta D(D)$ with the change in D , as discussed above.

V. ARRAY OF WALLS

To investigate the potential of avalanche suppression by closely placed walls, we undertook a series of simulations with arrays of equally spaced walls (Fig. 11). If the distance between the walls is small enough ($D < 4$) then system-wide

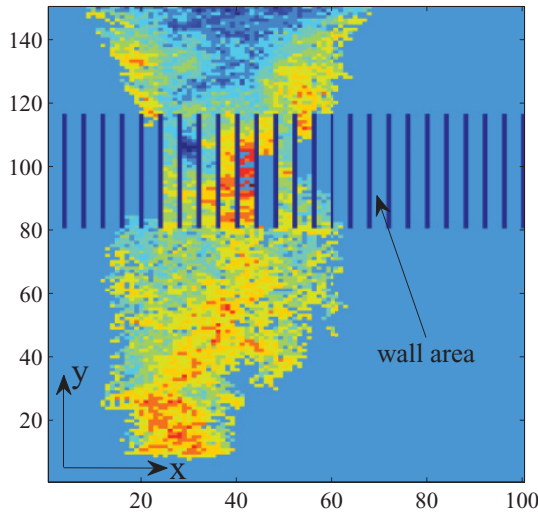


FIG. 11. (Color online) Example of an avalanche passing through the pile with the array of walls. Blue (upper dark gray part of the image) indicates regions where particles are removed, and red (lower part of the image) indicates regions where particles are added. The color saturation is a measure of the magnitude of change in vertical height. Note that the biggest changes are in the channels at $x = 30$, $y = 110$ (blue) and $x = 42$, $y = 100$ (red).

avalanche propagation through the middle area of the pile where the walls are placed is completely suppressed. However, after a certain amount of time, particles do propagate between the walls in the form of very small local avalanches, as may be seen from Fig. 11 where the avalanche is “most intense” (maximal change in height) at certain channels in the area between the walls. Channels behave quite independently: a minimal change in one channel can coexist with a maximal change in the neighboring channel.

Overall, the angle of the pile is steeper between the walls, see Fig. 12, which we attribute to avalanche suppression. In the

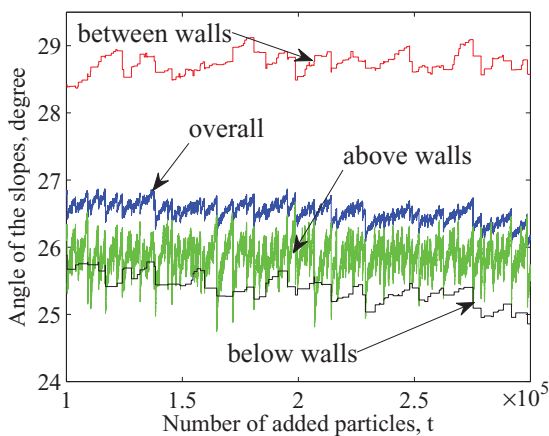


FIG. 12. (Color online) Average angles of the slope of the pile versus number of added particles t (time). Red is the angle between the walls, green is above the walls, black is below the walls, and blue is the average over the whole pile. Clearly, the slope is steepest between the walls. For clarity only the middle portion of the whole experimental duration is shown, between 1×10^5 and 3×10^5 particles added.

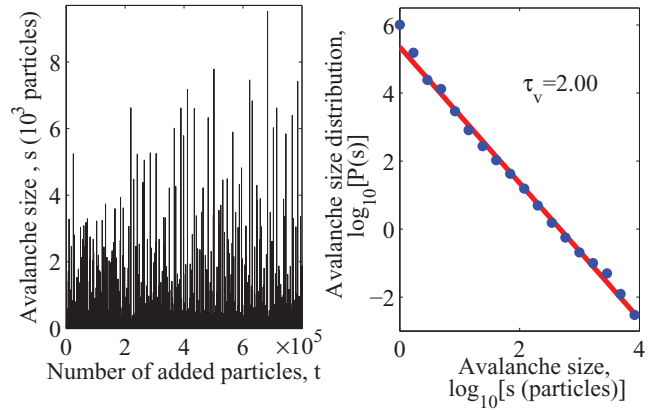


FIG. 13. (Color online) Avalanche size distribution with an array of walls present across the pile. Distance between walls is three sites. Simulation data points are shown by blue circles and the red solid line is the fit to $P(s) \sim s^{-\tau_v}$.

presence of the avalanche-suppressing walls, the pile adjusts to a steeper slope to retain a local SOC state. Above and below the walls the angles of the slope are initially equal, but during the course of the experiment the angle below the wall slightly decreases. This can be explained by the increasing roughness of the foot of the pile. The width of the foot increases with time, leading to angle decrease below the walls. It should also be noted that the angle above the walls fluctuates much more than that below the walls. Above the walls every small avalanche could change the surface of the pile and its average angle. Below the walls the surface changes only when an avalanche penetrates through the wall region, which is a relatively rare event.

Immediately below the wall area, there is a similar situation as at the top portion of the pile: there are no avalanches higher up. However, in contrast to the top of the pile, now occasionally many particles are added at virtually the same location. In any case, below the wall area, large avalanches reappear and the SOC state is recovered with the same avalanche size distribution as without the walls: $\tau_v \simeq 2$. The overall avalanche size distribution for the whole pile is shown in Fig. 13. The only improvement due to the presence of the walls is a local (at the walls) suppression of avalanches. Large, even system-wide, avalanches occur with a total maximum avalanche size only slightly smaller (by the factor 1.5) than without walls, taking into account the fact that the walls divide the whole pile surface into two parts. This observation supports the fact that SOC behavior is quite robust and is very difficult to suppress.

VI. CONCLUSIONS

A Casimir-like behavior in a granular pile has been simulated using a modified BTW model. Two parallel walls in the presence of fluctuations (avalanches) experience an interaction with the moving particles. Interactions between particles and walls are less frequent inside than outside the region between the walls, leading to an attractive force. This result is in agreement with the previous experimental observation of this effect [10] in an avalanching pile of rice. The attractive force decays with increasing separation between the walls; however, it does not directly decay to zero, as in the

experiment. In contrast, first a switching from attraction to weak repulsion is observed for intermediate distances. The repulsive force can be explained by multiple collisions of the same individual particles with the walls, when an avalanche is (partially) trapped between the walls. The magnitude of the repulsive force is rather small, which is probably why it was not observed experimentally.

We also explored the potential for avalanche suppression of an array of parallel walls. While indeed avalanches are

suppressed between the walls, normal avalanche behavior is quickly recovered below the walls. We conclude that SOC is very difficult to suppress.

ACKNOWLEDGMENTS

This work was supported by the Foundation for Fundamental Research on Matter (FOM) which is subsidized by the Netherlands Organization for Scientific Research (NWO).

-
- [1] P. Bak, C. Tang, and K. Wiesenfeld, *Phys. Rev. Lett.* **59**, 381 (1987).
 - [2] C. H. Scholz, *The Mechanics of Earthquakes and Faulting* (Cambridge University Press, Cambridge, England, 1991).
 - [3] S. Hergarten and H. J. Neugebauer, *Geophys. Res. Lett.* **25**, 801 (1998).
 - [4] B. Drossel and F. Schwabl, *Phys. Rev. Lett.* **69**, 1629 (1992).
 - [5] V. Frette, K. Christensen, A. Malthe-Sorensen, J. Feder, T. Jossang, and P. Meakin, *Nature (London)* **39**, 49 (1996).
 - [6] C. M. Aegerter, M. S. Welling, and R. J. Wijngaarden, *Europhys. Lett.* **65**, 753 (2004).
 - [7] P. Bak and K. Sneppen, *Phys. Rev. Lett.* **71**, 4083 (1993).
 - [8] M. Bartolozzi, D. B. Leinweber, and A. W. Thomas, *Physica A* **370**, 132 (2006).
 - [9] H. B. G. Casimir, *Proc. K. Ned. Akad. Wet.* **51**, 793 (1948).
 - [10] Y. Y. Villanueva, D. V. Denisov, S. de Man, and R. J. Wijngaarden, *Phys. Rev. E* **82**, 041303 (2010).
 - [11] P. Bak, C. Tang, and K. Wiesenfeld, *Phys. Rev. A* **38**, 364 (1988).
 - [12] S. S. Manna, *J. Phys. A* **24**, 363 (1991).
 - [13] A. Corral and M. Paczuski, *Phys. Rev. Lett.* **83**, 572 (1999).
 - [14] Yi-Chneg Zhang, *Phys. Rev. Lett.* **63**, 470 (1989).
 - [15] K. Christensen, A. Corral, V. Frette, J. Feder, and T. Jossang, *Phys. Rev. Lett.* **77**, 107 (1996).
 - [16] M. Bengrine, A. Benyoussef, A. El Kenz, M. Loulidi, and F. Mhirech, *Eur. Phys. J. B* **12**, 129 (1999).
 - [17] K. A. Lórinicz, Ph.D. dissertation Vrije Universiteit, 2008.